



Spike-Related Electrophysiological Identification of Cultured Hippocampal Excitatory and Inhibitory Neurons

Cosimo Prestigio¹ · Daniele Ferrante² · Pierluigi Valente^{2,3} · Silvia Casagrande² · Ennio Albanesi⁴ · Yuchio Yanagawa⁵ · Fabio Benfenati^{1,3} · Pietro Baldelli^{2,3} 

Received: 23 November 2018 / Accepted: 23 January 2019 / Published online: 12 February 2019
© Springer Science+Business Media, LLC, part of Springer Nature 2019

Abstract

Cultured hippocampal neurons represent the most widely used experimental substrate for *in vitro* electrophysiological studies. Nevertheless, in most cases, the nature of neuron under study is not identified as excitatory or inhibitory, or even worse, recorded neurons are considered as excitatory because of the paucity of GABAergic interneurons. Thus, the definition of reliable criteria able to guarantee an unequivocal identification of excitatory and inhibitory cultured hippocampal neurons is an unmet need. To reach this goal, we compared the electrophysiological properties and the localization and size of the axon initial segment (AIS) of cultured hippocampal neurons, taking advantage from GAD67-GFP knock-in mice, which expressing green fluorescent protein (GFP) in gamma-aminobutyric acid (GABA)-containing cells, allowed to unambiguously determine the precise nature of the neuron under study. Our results demonstrate that the passive electrophysiological properties, the localization and size of the AIS, and the shape and frequency of the action potential (AP) are not reliable to unequivocally identify neurons as excitatory or inhibitory. The only parameter, related to the shape of the single AP, showing minimal overlap between the sample-point distributions of the two neuronal subpopulations, was the AP half-width. However, the estimation of the AP failure ratio evoked by a short train of high-current steps applied at increasing frequency (40–140 Hz) resulted to be indisputably the safer and faster way to identify the excitatory or inhibitory nature of an unknown neuron. Our findings provide a precise framework for further electrophysiological investigations of *in vitro* hippocampal neurons.

Keywords Excitatory neurons · Inhibitory neurons · Action potential · Firing frequency · Half-width · Axonal initial segment

Introduction

The hippocampus plays fundamental functional roles in cognition, learning, and memory [1]. However, the complexity of

this structure makes it challenging to manipulate and analyze *in vivo*. One of the most well-established and widely used techniques for the study of hippocampal neurons is the primary dissociated cell culture system obtained from embryonic [2]

✉ Pietro Baldelli
pietro.baldelli@unige.it

Cosimo Prestigio
cosimo.prestigio@iit.it

Daniele Ferrante
daniele.ferrante@edu.unige.it

Pierluigi Valente
pierluigi.valente@unige.it

Silvia Casagrande
silvia.casagrande@unige.it

Ennio Albanesi
ennio.albanesi@iit.it

Yuchio Yanagawa
yuchio@gunma-u.ac.jp

Fabio Benfenati
fabio.benfenati@iit.it

¹ Center for Synaptic Neuroscience and Technology, Istituto Italiano di Tecnologia, 16132 Genoa, Italy

² Department of Experimental Medicine, School of Medicine and Pharmacy, University of Genoa, 16132 Genoa, Italy

³ IRCSS, Ospedale Policlinico San Martino, 16132 Genoa, Italy

⁴ Department of Neuroscience and Brain Technologies, Istituto Italiano di Tecnologia, 16163 Genova, Italy

⁵ Department of Genetic and Behavioral Neuroscience, Gunma University Graduate School of Medicine, Maebashi 371-8511, Japan

or postnatal [3] rat or mouse brain. This approach allows neurons to be cultured in vitro in a far less complex environment than that used in vivo, making them highly accessible to physiological and pharmacological manipulations. In culture, hippocampal cells develop by expressing neuronal antigens and acquiring mature neuronal morphologies, including high differentiation of the axons, increasing the complexity of dendritic tree, and synapse formation and maturation. This methodology, coupled with advanced electrophysiological technologies and manipulation of gene expression, is suitable for dissecting out various aspects of molecular and cellular mechanisms that underlie long-term processes of functional differentiation and degeneration of the neuronal networks. Cultured neuronal networks allow us to study relatively late events such as synaptogenesis and various forms of synaptic and intrinsic plasticity that develop in response to long-lasting (hours/days) electrical or chemical treatments that would be otherwise not possible in acute brain slices.

In this respect, dissociated hippocampal neurons obtained from rat/mouse embryos (E16–18) or pups (P0–3) unquestionably represent the most widely used experimental substrate. Two major classes of neurons constitute the hippocampal neuronal networks: the excitatory glutamatergic and the inhibitory GABAergic neurons. Nevertheless, in most cases, the different neuronal subtypes are not exactly discerned, or are considered roughly all excitatory neurons, because it is widely accepted that excitatory glutamatergic neurons represent approximately 80% of the entire neuronal population.

Moreover, even when a distinction is attempted, it is often based on a non-specific morphological analysis of the soma shape and/or dendritic tree complexity. This approach is obviously subjective and poorly reproducible. However, the identification of the true excitatory or inhibitory nature of the specific neuron under analysis is mandatory for the correct interpretation of the electrophysiological data.

Most studies describing changes in frequency, amplitude, and kinetics of spontaneous miniature excitatory or inhibitory postsynaptic currents (mEPSCs or mIPSCs) are conducted on neurons whose excitatory or inhibitory nature is uncertain. Nevertheless, it is now clear that the postsynaptic nature of the neuron reached by a specific synaptic contact determines the strength and plasticity properties of the synapse, and its sensitivity to both endogenous and exogenous modulators [4].

The aim of this paper is the development of an easy and rapid approach to unambiguously distinguish glutamatergic from GABAergic cells in primary cultures of hippocampal neurons. We analyzed passive and active membrane properties, localization, and size of the axon initial segment (AIS) in GFP-negative (GFP⁻) glutamatergic and GFP-positive (GFP⁺) GABAergic hippocampal neurons obtained from knock-in mice expressing GFP under the control of the glutamate decarboxylase 67 (GAD67) endogenous promoter [5, 6]. We demonstrate that the action potential (AP) half-width and the

firing frequency reached in response to a train of repetitive stimulation represent the two main parameters, related to the intrinsic properties of the neurons, allowing a fast and reliable identification of the excitatory or inhibitory nature of in vitro hippocampal neurons.

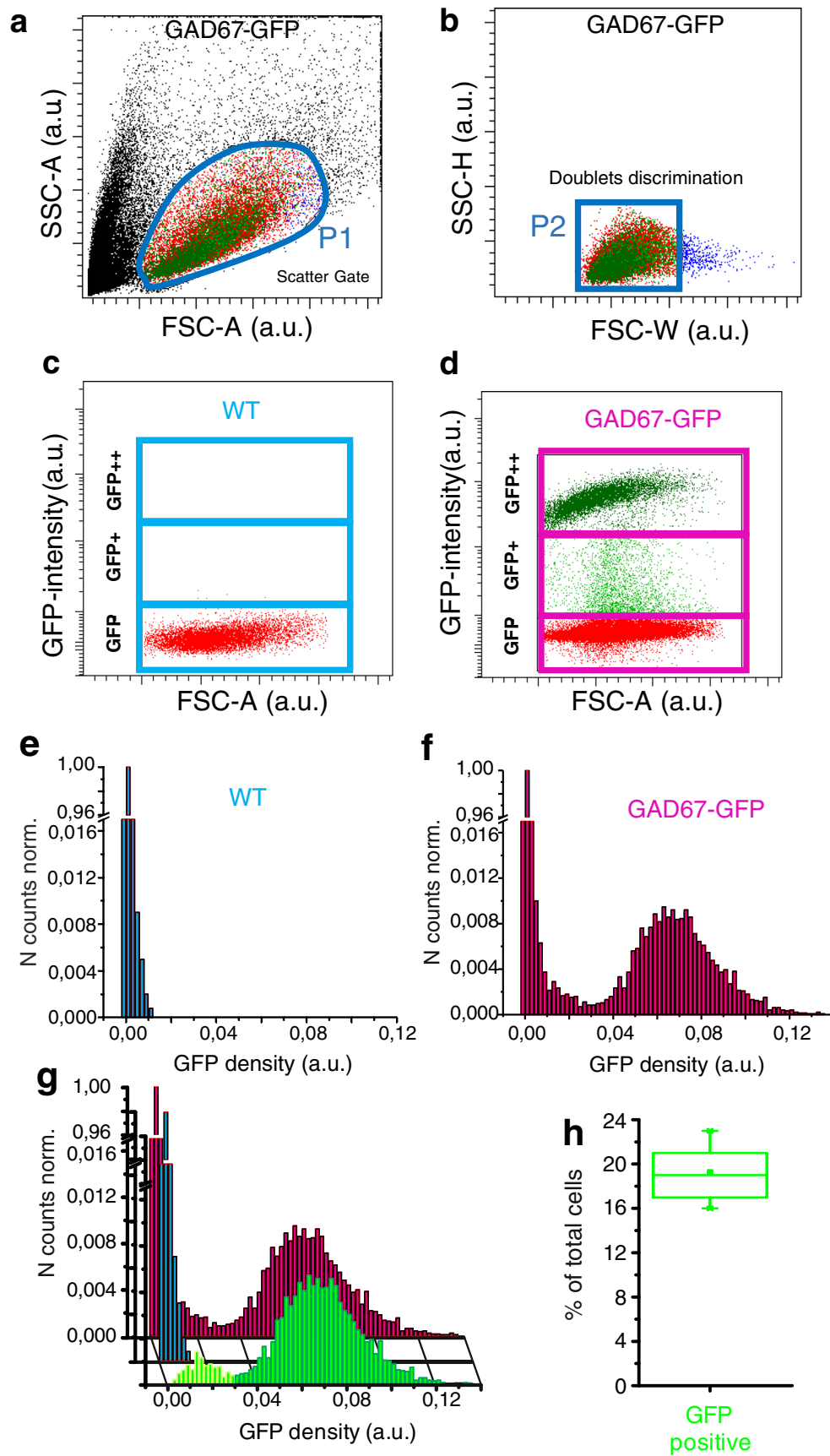
Results

Florescent-Activated Cell-Sorting Analysis of GAD67-GFP Hippocampal Neurons

The use of GAD67-GFP mice offers the advantage to optically identify live GFP⁺ GABAergic interneurons and GFP⁻ glutamatergic excitatory neurons. Previous data have shown that the large majority of the GFP⁺ cells express GABAergic markers in GAD67-GFP knock-in mice [5, 7, 8] and patch-clamp recording showed that all GFP⁺ neurons were functionally GABAergic [9]. However, our recent results [10] revealed that in primary GAD67-GFP hippocampal neurons, a fraction of excitatory dentate gyrus granule neurons are moderately GFP⁺ because of the ability to express significant levels of GAD67, as also previously observed by others [11–13].

To clarify this aspect, we used fluorescence-activated cell sorting (FACS) to analyze cells obtained from the enzymatic and mechanical dissociation of GAD67-GFP and wild-type (WT) littermates (P0–P1) hippocampi. In the plot of the forward scatter area (FSC-A; proportional to the event size) vs the side scatter area (SSC-A; proportional to the event inner-complexity), each dot represents a single flow cytometry signal (counts), represented by cells, cellular debris, or cell clumps/doublets passing through the laser beam (Fig. 1a). The region of interest (ROI) named P1 eliminates most of the cellular debris (characterized by very low FSC-A values) and part of the cell clumps (characterized by large FSC-A and SSC-A values). A further ROI (P2) was depicted on the scatter plot of the side scatter width (SSC-W) vs the side scatter

Fig. 1 FACS analysis of GAD67-GFP primary hippocampal neurons. **a** Scatter plot of the forward scatter area (FSC-A) vs the side scatter area (SSC-A). The blue line defines the region of interest (ROI) named P1, selecting putative single cells subsequently plotted in panel **b**. **b** Scatter plot of the side scatter width (SSC-W) vs side scatter height (SSC-H) of the putative cells selected by P1 ROI. A further ROI (P2) was depicted on this scatter plot to completely eliminate cell clumps and cell doublets characterized by high SSC-W. The described approach was the same used on both WT and GAD67-GFP to isolate events only representing single cells. **c, d** Representative final scatter graphs of the cell size (FSC-A) vs GFP fluorescent intensity (GFP-A) for both WT (**c**) and GAD67-GFP (**d**) cells. **e–f** Histograms of the distribution of the fluorescence density (fluorescence intensity/FSC-A) values for both WT (**e**) and GAD67-GFP (**f**) cells. **g** Graph showing the subtraction of the WT profile (blue) from the GAD67-GFP histogram (pink), highlighting the distribution of the GFP-positive cells (green). **h** Box plot showing the mean percentage of GFP⁺ cells in our preparations ($n = 4$ different cell culture preparations)



height (SSC-H) of the P1 counts, to eliminate the further cell clumps/doublets characterized by high SSC-W values (Fig. 1b).

The described approach was used on both WT (Fig. 1c) and GAD67-GFP neurons (Fig. 1d) to isolate single-cell events that were plotted in a final scatter graph, showing the cell size (FSC-A) vs GFP fluorescent intensity (GFP intensity). For a more accurate distinction of the GFP+ and GFP- cells, the GFP fluorescence intensity was divided by the respective FSC-A value (cell size), obtaining an estimation of the GFP density for each cell, and subsequently normalized to the maximum fluorescence density. The distribution of the GFP fluorescence density of cells obtained from WT hippocampi (Fig. 1e) consisted in sharp Gaussian curve showing very low levels of autofluorescence (always below 0.012 a.u.). On the contrary, the distribution of the fluorescence density of GAD67-GFP cells (Fig. 1f) was bimodal, with a second Gaussian curve centered at higher GFP density values. After subtraction of the WT profile from the GAD67-GFP histogram, a distribution histogram of the GFP+ cells was obtained. This analysis showed that GFP+ cells represent about 20% of the total number of cells (neurons and glial cells) and display fluorescence densities varying from 0.02 to 0.1 (a.u.), with a fivefold range between the extremes (Fig. 1g, h). This result demonstrates the existence of a significant heterogeneity in the expression of GFP, and thereby of GAD67.

Characterization of Cultured GAD67-GFP Hippocampal Neurons

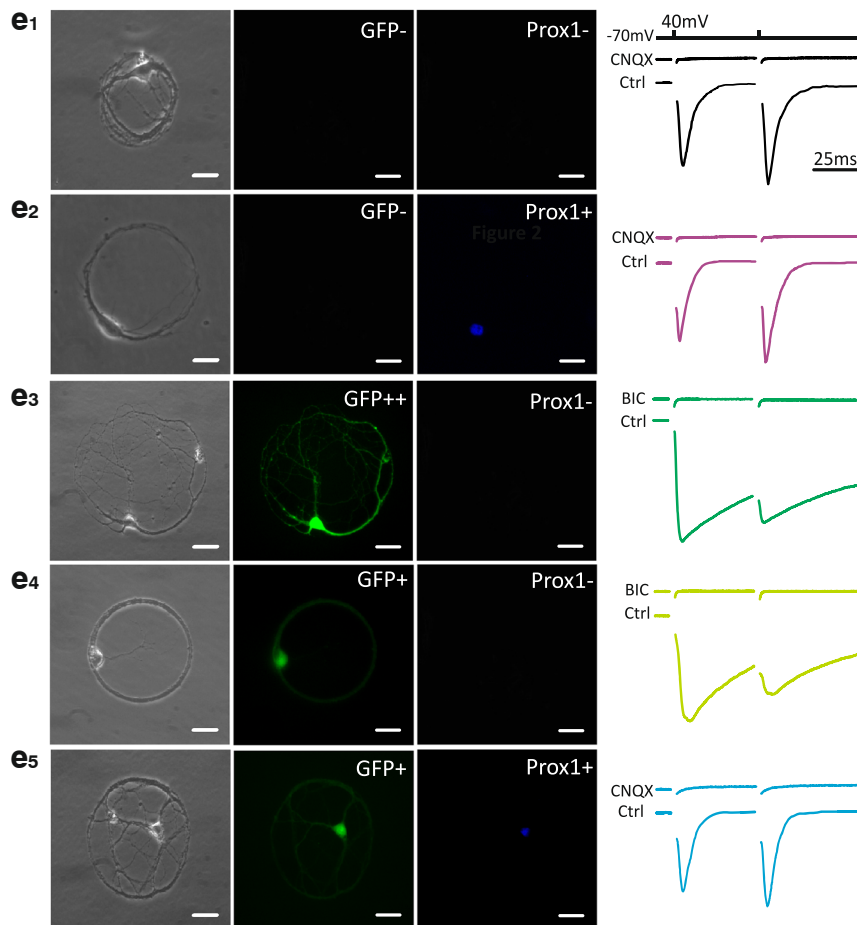
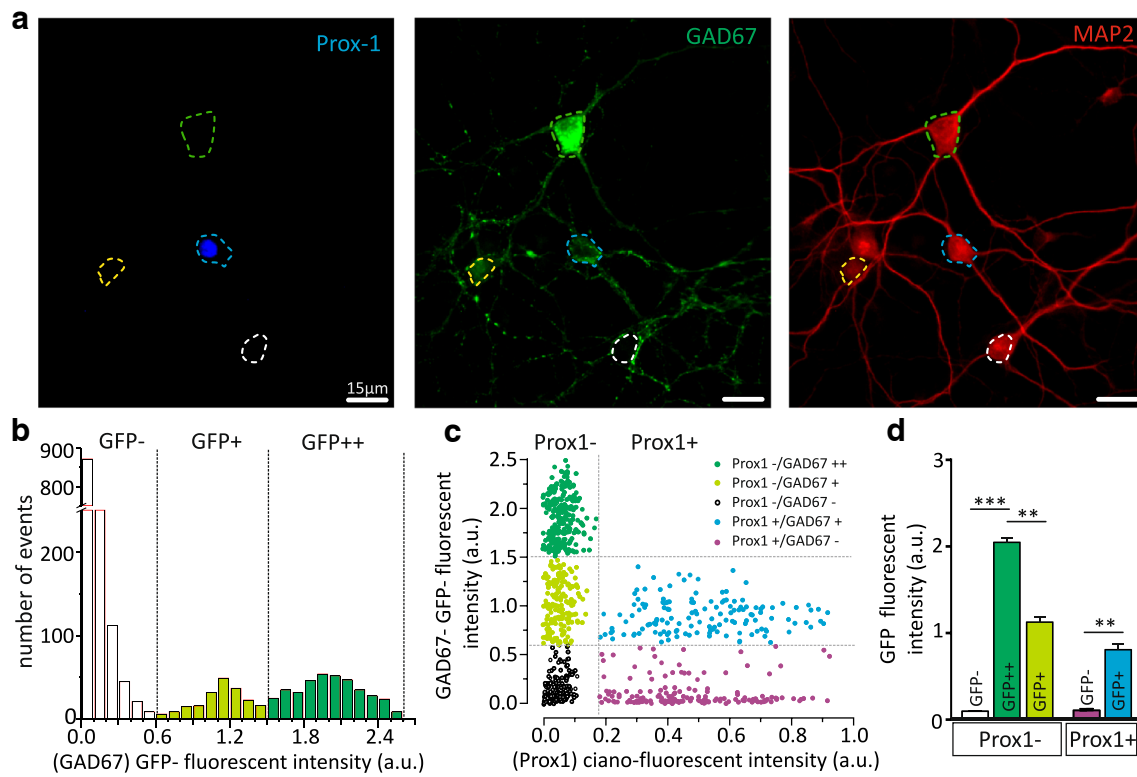
In order to precisely identify excitatory or inhibitory cultured hippocampal neurons obtained from GAD67-GFP pups (P0-P1), we used both immunocytochemistry of low-density hippocampal neurons and patch-clamp recordings of synaptic transmission in autaptic hippocampal neurons.

Low-density hippocampal neurons (12–16 div) were immunostained for MAP-2, a neuron-specific marker, and Prox1, a transcription factor selectively expressed in mature granule cells of the dentate gyrus [14], while the expression of GAD67 was evaluated based on the endogenous fluorescence of GFP (Fig. 2a). Since both the GFP and the GAD67 genes in the GAD67-GFP knock-in mice are identically controlled, the parallel GFP protein expression accurately reflects the expression of GAD67 in GABAergic neurons [15, 16]. As expected, the distribution histogram of the GAD67-GFP intensity revealed the existence of three distinct neuronal subpopulations. In addition to the vast majority of GFP- (putatively excitatory) neurons (GFP intensity < 0.6 a.u.: GFP-), other two neuronal subpopulations clearly appeared, constituted by neurons moderately (0.6 < GFP intensity < 1.5 a.u.; GFP+) or intensively (1.5 < GFP intensity < 2.5 a.u.; GFP++) positive

Fig. 2 Heterogeneity of the neuronal populations in GAD67-GFP primary hippocampal neurons. **a** Representative confocal images of low-density hippocampal neurons stained for Prox1 (left) and MAP2 (right). The middle panel shows GFP expressed in the soma and dendrites of GAD67-GFP neurons. In these images, four subpopulations of neurons can be identified: (i) Prox1-negative, GAD67-GFP-intensively positive neurons (green circle); (ii) Prox1-negative, GAD67-GFP-moderately positive neurons (yellow circle); (iii) Prox1-positive, GAD67-GFP-negative neurons (blue circle); and (iv) Prox1-negative GAD67-GFP-negative neurons (white circle). Scale bar, 15 μ m. **b** Accordingly, the distribution histogram of the GFP fluorescent intensity, three distinct neuronal subpopulations can be identified: (i) a vast majority of GAD67-negative cells (GFP-; GFP intensity < 0.6 a.u.), (ii) neurons moderately positive to GAD67-GFP (GFP+; 0.6 < GFP intensity < 1.5 a.u.), and (iii) neurons intensively positive to GAD67-GFP (GFP++; 1.5 < GFP intensity < 2.5 a.u.). **c** Scatter plot showing the distribution of the staining intensities of Prox1 vs GAD67-GFP in low-density neurons. Each spot represents an individual neuron. Five subpopulations are clearly identified: (i) inhibitory neurons strongly positive to GAD67-GFP and negative to Prox1 (dark green spots), (ii) additional putative inhibitory neurons moderately positive to GAD67-GFP and negative to Prox1 (light green spots), (iii) excitatory neurons negative for GAD67 and Prox1 (black spots), (iv) putative excitatory granule cells moderately positive to GAD67-GFP and positive for Prox1 (blue spots), and (v) putative excitatory granule cells negative to GAD67-GFP and positive for Prox1 (violet spots). **d** Bar plot of the mean GAD67-GFP fluorescence intensity of the five neuronal subpopulations described in **c**. Data are shown as means \pm SEM. * P < 0.05, ** P < 0.01, *** P < 0.001, one-way ANOVA/Tukey's multiple comparison test. **(e1-5)** On the left, representative phase contrast microphotographs (left panels) and fluorescence images of autaptic neurons analyzed for GAD67-GFP (middle panels) and Prox1 (right panels). On the right, the same autaptic neurons were previously patch-clamped to evoke postsynaptic currents (PSCs) (stimulation protocol in the inset) that were pharmacologically characterized using CNQX (10 μ M) and BIC (30 μ M). The stimulation artifacts were blanked for clarity. From top to bottom: **(e1)** an excitatory autaptic neuron negative for GAD67 and Prox1, whose ePSCs were fully blocked by CNQX; **(e2)** an autaptic granule cell negative for GAD67 and positive for Prox1, whose ePSCs were fully blocked by CNQX; **(e3)** an inhibitory autaptic neuron highly positive for GAD67 and negative for Prox1, whose ePSCs were fully blocked by BIC; **(e4)** an inhibitory autaptic neuron moderately positive for GAD67 and negative for Prox1, whose ePSCs were fully blocked by BIC; **(e5)** a granule cell moderately positive for GAD67 and positive for Prox1, whose ePSCs were fully blocked by CNQX. Scale bar, 15 μ m

for GAD67 (Fig. 2b). Then, we investigated expression of Prox1, a transcription factor constitutively expressed in the dentate gyrus granule cells.

The study of GAD67-GFP vs Prox1-CFP intensities highlighted a more complex scenario (Fig. 2c). Indeed, while GAD67-intensively positive neurons were all Prox1-negative, in both GAD67-negative neurons and GAD67-moderately positive neurons, we identified the presence of Prox1-positive neurons (Fig. 2c). Thus, the GFP expression level clearly distinguishes the excitatory/inhibitory nature only for those neurons that are negative or intensively positive for GFP. Indeed, a subpopulation of neurons moderately GFP-positive exists that comprises a mix of excitatory granule cells and inhibitory GABAergic neurons (Fig. 2d).



Next, we studied synaptic transmission in GAD67-GFP autaptic cultured hippocampal neurons (10–14 div) where Prox1 expression was retrospectively evaluated by immunoassay. Autaptic neurons offer the fundamental advantage of recording synaptic currents from a defined and homogeneous population of synapses. Patch-clamp recordings were used to record evoked excitatory or inhibitory postsynaptic currents (eEPSCs or eIPSCs) identified by the alternate use of the AMPA receptor antagonist, CNQX (10 μ M), or the GABA_A receptor blocker, bicuculline (BIC; 30 μ M) (Fig. 2e). Virtually, all GFP-negative neurons showed CNQX-sensitive eEPSCs (Fig. 2e₁, e₂) and retrospective immunoassay revealed that most of these neurons were Prox1-negative (Fig. 2e₁) while the rest were Prox1-positive (Fig. 2e₂); all GFP-intensively positive neurons showed BIC-sensitive eIPSCs and were Prox1-negative (Fig. 2e₃); the 70% of GFP-moderately positive neurons ($0.6 < \text{GFP intensity} < 1.5$ a.u.) showed BIC-sensitive eIPSCs and were Prox1-negative (Fig. 2e₄) while the remaining 30% displayed CNQX-sensitive eEPSCs and were Prox1-positive (Fig. 2e₅).

In summary, these results confirm that GFP-negative (GFP⁻) and GFP-intensively positive (GFP⁺⁺) neurons are excitatory and inhibitory neurons, respectively, while GAD67-moderately positive neurons (GFP⁺) are composed by both excitatory granule cells and GABAergic inhibitory neurons.

Waveform of the Single Action Potential in Excitatory and Inhibitory Cultured Hippocampal Neurons

Thus, the identification of excitatory and inhibitory neurons in low-density GAD67-GFP hippocampal cultures was based on their negativity or strong positivity to GFP, while, in the case of GAD67-moderately positive neurons, on the basis of their autaptic eEPSCs. Thanks to this strategy, we were able to obtain an electrophysiological characterization of the firing properties of all cultured hippocampal neurons with the goal of identifying those electrophysiological biomarkers that can allow reliable identification of excitatory and inhibitory hippocampal neurons in the absence of GAD-GFP labeling.

Both conventional low-density and autaptic neuron cultures (12–16 div) were analyzed by patch-clamp recordings in current-clamp configuration. Neurons were injected with 10 mV increment current steps, lasting 1 s with inter-pulse intervals of 2 s. For consistency, current steps were delivered from a membrane potential of -80 mV, maintained by constant current injection (Fig. 3a).

The analysis of the passive membrane properties did not provide any useful parameters that would allow a quick and certain distinction between neurons. Indeed, the membrane capacitance (C_m) and the resting potential (V_{rest}) were not significantly different between the two groups.

Although input resistance (R_{in}) was significantly lower in inhibitory neurons, the values showed a clear overlap between the two neuronal populations (Fig. 3b). As extensively reviewed [17], the R_{in} of hippocampal GABAergic interneurons is very heterogenous, ranging from 100 to 400 M Ω . Even more heterogenous is the R_{in} of excitatory neurons, resulting from the average of the low R_{in} of large pyramidal neurons [18] with the higher R_{in} of the very small dentate gyrus granule cells [19].

Hence, we analyzed the waveforms of the first AP evoked during a minimal current injection near the firing threshold [15] (Fig. 3c). The maximum rising slope (max dV/dt) (Fig. 3d), the maximal repolarizing slope (Fig. 3e), the AP peak (Fig. 3f), and the afterhyperpolarization (AHP; Fig. 3g) were all significantly different between the two populations, but with a clear overlap of the distribution of data points that does not allow to unambiguously identify the excitatory or inhibitory nature of the neurons. The only parameter showing minimal overlap between the individual data distributions was the AP half-width (2.66 ± 0.12 and 1.036 ± 0.06 ms, for excitatory and inhibitory neurons, respectively; Fig. 3h). Collectively, these data testify that GABAergic hippocampal interneurons fire shorter lasting APs than glutamatergic hippocampal neurons.

All AP parameters, describing changes of the waveform of the single AP, in excitatory and inhibitory neurons, are summarized in Table 1.

Phase-Plane Plot Analysis

Although action potentials initiate at the AIS, they are generally investigated by patch-clamp recordings in the neuronal cell body [20–23]. To investigate in more detail the difference in the intrinsic properties of excitatory and inhibitory hippocampal neurons, we studied the AP initiation at the AIS by examining the onset kinetics of somatically recorded APs.

It has been demonstrated that the membrane potential change rate (i.e., the first derivative dV/dt) vs voltage, commonly named the phase-plane plot, exhibits a two-component biphasic increase rate during spike generation. The first component is due to spike initiation at the AIS that generates a sudden voltage increase from baseline called “kink” [22]. The invasion of the soma by the AIS spike generates a delayed and larger second component of the phase-plot (the “somatodendritic spike”) [24, 25] reaching the AP peak.

The shape of the averaged AP (Fig. 4a), evoked by constant current injection that maintains the holding voltage just over the voltage threshold, was analyzed by using the plot of the time derivative of voltage (dV/dt) vs time (Fig. 4b) and vs voltage (Fig. 4c), allowing a better resolution of the fast change in kinetics of AP initiation that depends on voltage-gated Na⁺ channel (VGNaCh) conductance.

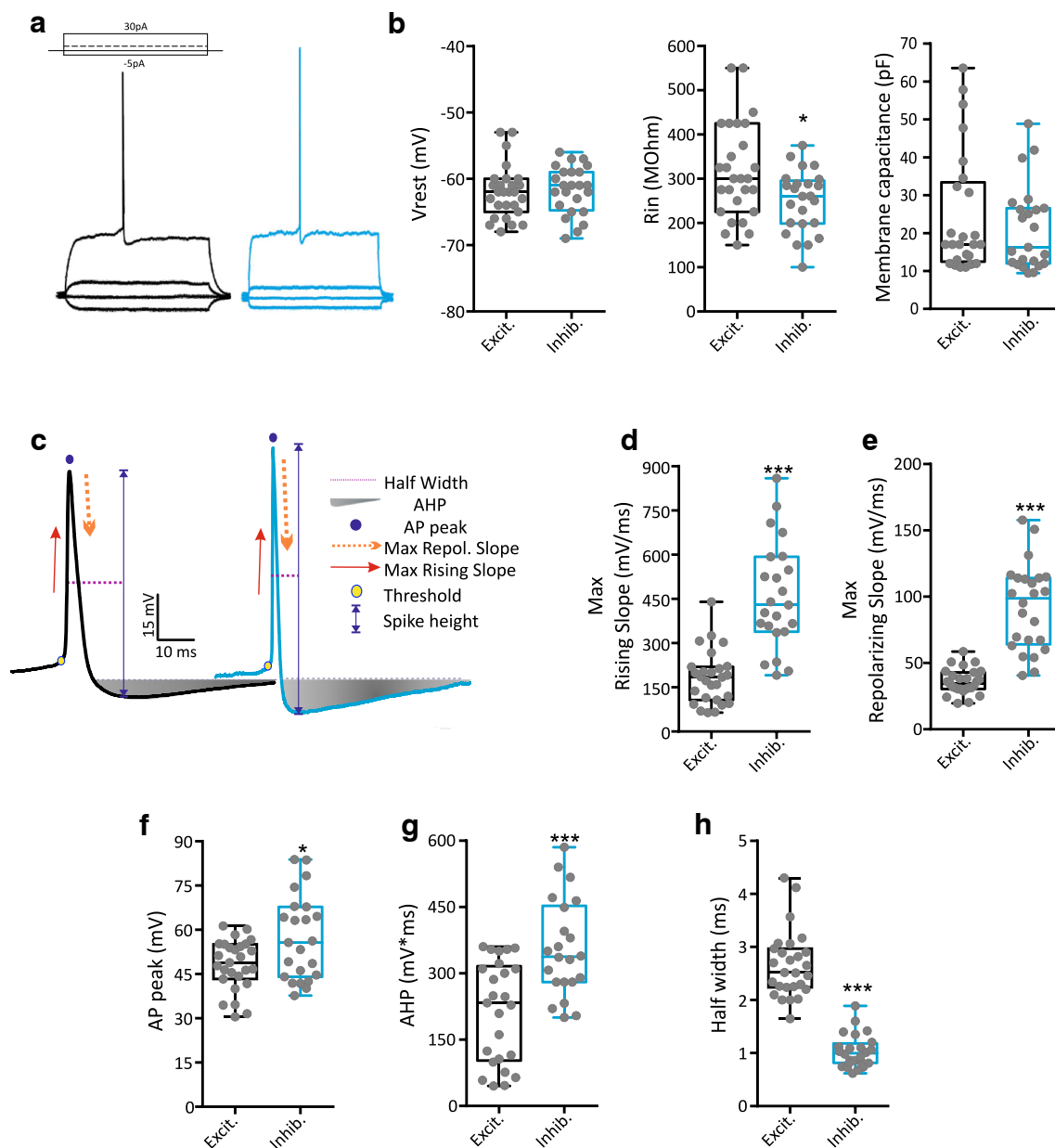


Fig. 3 Analysis of the passive and active properties of hippocampal neurons. **a** Representative current-clamp recordings obtained by injecting 4 current steps lasting 1 s (inset) in excitatory and inhibitory neurons. **b** Box plots of the resting membrane potential (V_{rest}), membrane input resistance (R_{in}), and membrane capacitance (C_m) for both phenotypes. **c** Representative shapes of the first AP elicited by minimal current injection showing the main AP parameters measured in excitatory (black trace) and inhibitory (blue trace) neurons. **d-e** Box plots of maximum rising slope and maximal repolarizing slope of APs evoked in both cell types. **f-h** Box plots of AP peak, afterhyperpolarization (AHP), and half-width values. All AP parameters were obtained from the analysis of recordings of $n = 30$ cells for both conditions. Mann-Whitney U test * $P < 0.05$; ** $P < 0.01$; *** $P < 0.001$

The membrane potential slope (dV/dt) vs membrane potential showed strong differences between excitatory and inhibitory neurons. The representative phase-plots reveal that the “kink” was present in all excitatory and inhibitory neurons but it was significantly lower in excitatory neurons (Fig. 4c). To quantify such differences, we measured the slope of the phase plot at the Y-axis value of 4 mV/ms (Fig. 4d). Such a parameter, termed “phase slope,” has been used to measure the steepness of APs at their onset

and inhibitory (blue trace) neurons. **d-e** Box plots of maximum rising slope and maximal repolarizing slope of APs evoked in both cell types. **f-h** Box plots of AP peak, afterhyperpolarization (AHP), and half-width values. All AP parameters were obtained from the analysis of recordings of $n = 30$ cells for both conditions. Mann-Whitney U test * $P < 0.05$; ** $P < 0.01$; *** $P < 0.001$

[25–27]. Consistently, the phase slope was significantly lower in excitatory neurons than in inhibitory neurons (Fig. 4e). The phase-plane plot was also used to better resolve the voltage threshold, defined as the first voltage value at which dV/dt exceeded 4 mV/ms. Also, in this case, the comparison of both phenotypes highlighted a significant difference in the voltage threshold, although not so large to be used as a biomarker for the two neuronal sub-populations (Fig. 4f).

Table 1 Electrophysiological parameters describing passive and active membrane properties of excitatory and inhibitory primary hippocampal neurons

	Excitatory neurons	Inhibitory neurons	<i>p</i> value	Significance
Vresting (mV)	−62.04 ± 0.76	−61.67 ± 0.73	0.7299	ns
Rin (MΩ)	316.7 ± 20.76	249.4 ± 14.31	0.0121	*
Cm (pF)	24.54 ± 3.20	21.12 ± 2.32	0.5254	ns
Rheobase (pA)	125.9 ± 11.20	112.5 ± 7.40	0.3349	ns
Vthreshold (mV)	−31.51 ± 0.84	−34.58 ± 0.63	0.0069	**
Max rising slope (mV/ms)	181.5 ± 17.33	458.8 ± 37.74	4.65691E-07	***
Half-width (ms)	2.66 ± 0.12	1.036 ± 0.06	1.22415E-14	***
AP peak (mV)	48.16 ± 1.64	57.09 ± 2.9	0.013	*
Max repol. slope (mV/ms)	35.84 ± 1.81	92.27 ± 6.61	9.17917E-09	***
AHP (ms*mV)	214.5 ± 22.85	355 ± 23.47	9.51642E-05	***
Phase slope (ms ^{−1})	10.02 ± 0.38	15.39 ± 0.69	1.39206E-07	***
Inst. firing freq. (Hz; at 250pA)	29.72 ± 2.44	59.79 ± 4.51	1.5028E-06	***
Mean firing freq. (Hz; at 250 pA)	18.96 ± 1.17	41.47 ± 1.65	4.05915E-14	***
% of failures (train at 140 Hz)	11.67 ± 1.05	76.9 ± 1.4	5.15165E-31	***

Data are expressed as means ± SEM ($n \geq 30$ for both neuronal subpopulations. * $P < 0.05$, ** $P < 0.01$, *** $P < 0.001$; unpaired Student's *t* test or Mann-Whitney *U* test. ns, non-significant)

The Axon Initial Segment of Primary Excitatory and Inhibitory Hippocampal Neurons

It is known that VGNaChs are localized at the AIS through interactions with the scaffolding protein Ankyrin G (AnK G) [27, 28] and the accumulation of these channels at this level makes it the lowest threshold site for AP initiation [29, 30]. Thus, we asked whether the functional differences observed in neuronal excitability and the marked changes in the “phase slope” could be associated with an altered organization of AIS in excitatory and inhibitory neurons. To assess this, we analyzed the length and location of the AIS in primary hippocampal neurons (14–16 div) by confocal microscopy (Fig. 5a). Immunostaining for AnK G showed that the AIS length was shorter in inhibitory neurons compared to excitatory neurons (Fig. 5b, d), while the same based on anti-Na_v-staining was not significantly affected (Fig. 5c, e). Consistent with the results obtained with AnK G staining, inhibitory neurons showed the AIS start more distant from the cell body and the AIS end closer to the soma when compared to excitatory neurons (Fig. 5d), while the AIS start/end of Na_v-staining did not show any change between the two neuronal populations (Fig. 5e).

Firing Frequency of Cultured Excitatory and Inhibitory Hippocampal Neurons

Cell firing properties in response to electrotonic current step injections are frequently used to aid neuronal classification [31]. In this context, we have studied the firing frequency by delivering constant current pulses (1 s duration) of increasing amplitude (10 pA steps) and measuring the resulting AP firing rate in the two phenotypes under study (Fig. 6a–c). The mean

firing rate vs injected current clearly revealed that the inhibitory neurons displayed a higher evoked mean firing frequency with a difference reaching its maximum at the largest current injections (>250 pA) (Fig. 6c) when compared to excitatory neurons. However, the wide distribution of individual firing rates evoked at 250 pA makes this parameter unsuitable for a certain neuronal identification. We also measured the mean instantaneous frequency evoked at 250 pA, still obtaining results unable to distinguish excitatory from inhibitory neurons (Fig. 6b).

The unsatisfactory results obtained evoking AP with long-lasting (1 s) depolarizing current steps are probably due to the existence of numerous subclasses of interneurons that deviate from the typical “fast-spiking” behavior and exhibit a variety of spiking phenotypes (“adapting” or “bursting” behaviors).

To overcome this problem, we developed a stimulation protocol based on short-lasting (2.5 ms) supra-threshold current injection pulses, administered at frequencies ranging from 40 to 140 Hz (Fig. 6d). The supra-threshold current value was set at 100 pA over the minimal current able to evoke an AP for each step of a stimulation train at 10 Hz.

For each stimulation frequency, the percentage of elicited APs over the total number of stimuli was calculated in excitatory and inhibitory neurons. Both neuronal populations were able to fire 100% of APs with no significant failures at 40 Hz. However, at higher frequencies, all excitatory neurons displayed a progressively increasing amount of failures, while inhibitory neurons were able to efficiently cope with higher stimulation frequencies (80–140 Hz) with lower percentages of failures (Fig. 6d, e). In particular, at the highest stimulation frequencies (120 and 140 Hz), the distribution of the individual occurrence of failures showed the sharpest separation, indicating that this simple and fast stimulation protocol offers a

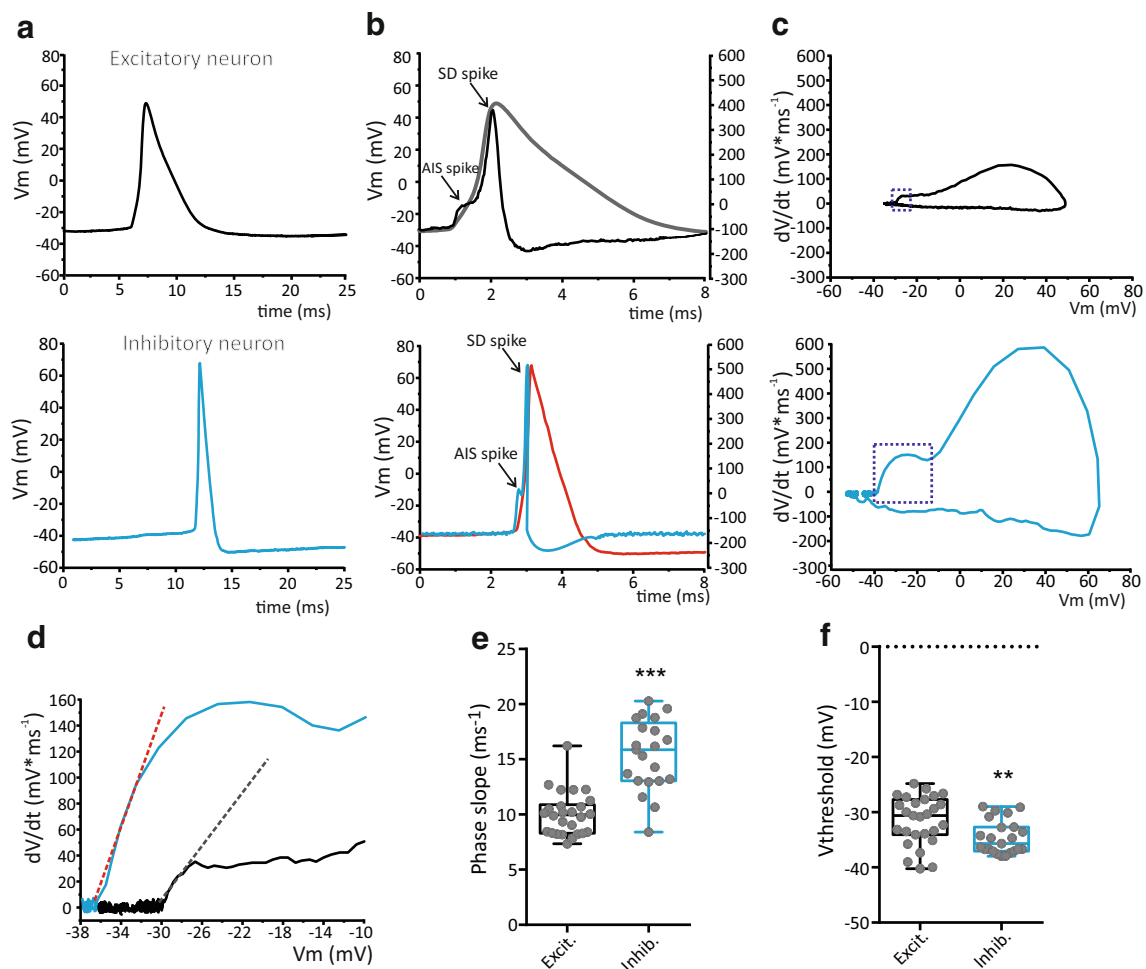


Fig. 4 Kinetics of AP initiation in excitatory and inhibitory neurons. **a** Representative APs recorded in excitatory (*upper panel*) and inhibitory (*lower panel*) neurons. APs were evoked by minimal current injection in both phenotypes. **b** AP shown in **a** (*gray/red traces*) are superimposed on the time course of the first derivative of the membrane voltage (dV/dt ; *black/blue traces*). The first arrow shows the rapid activation of the “AIS spike,” named “kink,” due to initiation of AP at the AIS. The second arrow shows the AP backpropagation to the somatodendritic

compartment, “SD spike.” **c** Plots of the first derivative of the membrane voltage (dV/dt) vs membrane voltage (V_m) (phase-plots) of the APs shown in **a** for excitatory (*upper panel*) and inhibitory (*lower panel*) neurons. **d** Plots of dV/dt vs V_m in the range between -38 and -10 mV to highlight the difference in the rate of rise AP initiation (phase slope) observed in both phenotypes. **e**, **f** Box plot of the phase slope (**e**) and of the voltage threshold (**f**) measured in excitatory ($n = 30$) and inhibitory ($n = 30$) neurons. $**P < 0.01$, $***P < 0.001$, Mann-Whitney U test)

safe and certain identification of the excitatory or inhibitory nature of cultured hippocampal neurons.

Discussion

A critical drawback of the electrophysiological studies of primary neuronal cultures is related to the absolute loss of the original cytoarchitecture that makes very difficult the morphological identification of the excitatory and inhibitory neuronal subpopulations. This explains why, over the years, many electrophysiological studies have been conducted on neurons of unknown nature.

In the vast majority of manuscripts published in high impact journals, synaptic transmission is investigated by recording spontaneous TTX-insensitive (“miniature”) postsynaptic

currents/potentials, and only a small percentage of these studies identify the excitatory or inhibitory nature of the postsynaptic neuron. Thus, the development of an easy and rapid electrophysiological method to unequivocally distinguish the exact nature of the patched neurons would be extremely helpful.

This scenario can be better understood if we consider the limitations of the various methods commonly used to define the excitatory/inhibitory nature of a neuron. The most widely used method is retrospective, based on the immunocytochemistry. The neuron is recorded using a patch pipette previously filled with a fluorescent tracer. Subsequently, neurons are fixed and subjected to immunocytochemistry using antibodies recognizing specific markers selectively expressed in excitatory glutamatergic or in inhibitory GABAergic neurons. This method, although safe and simple, has two major drawbacks,

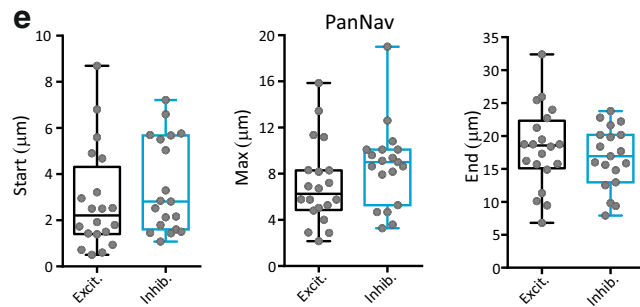
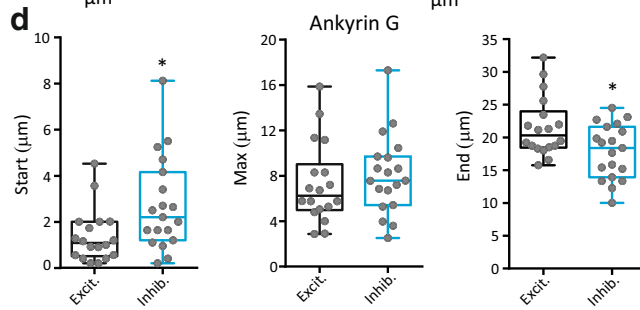
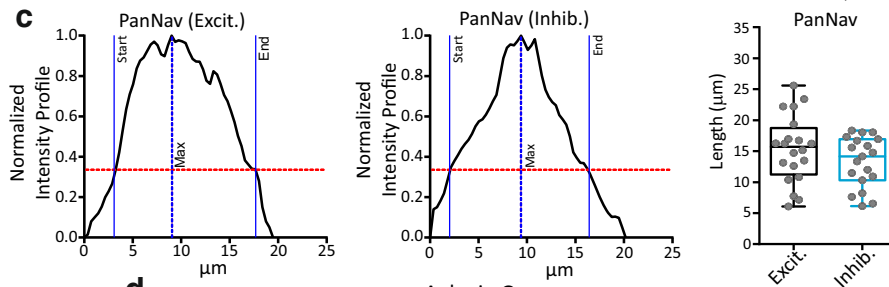
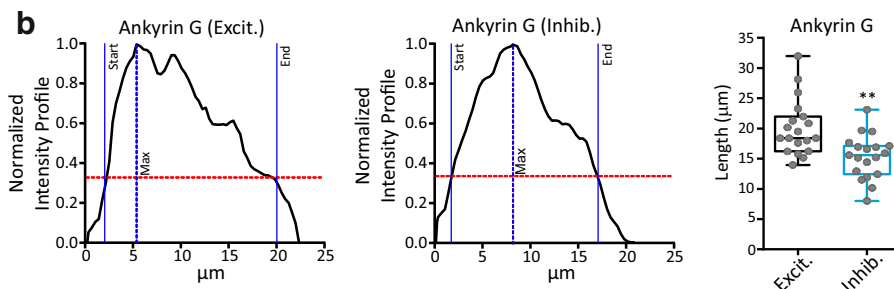
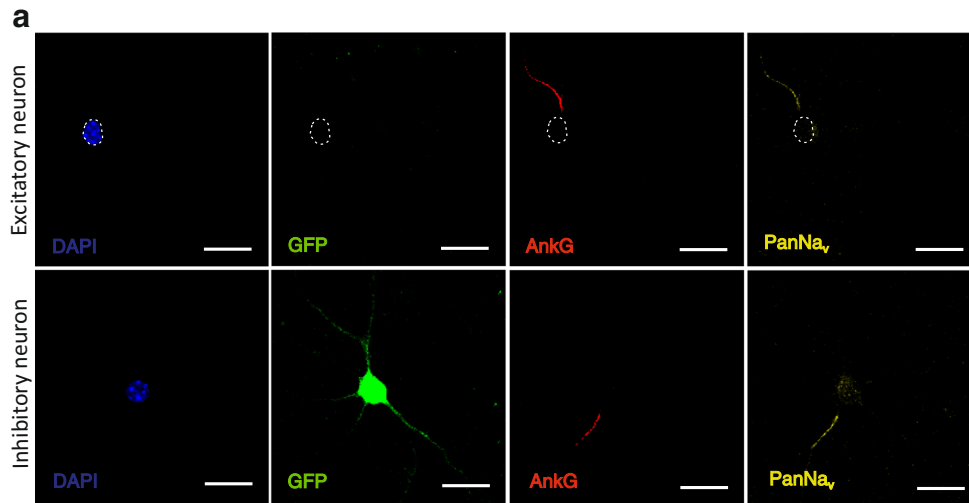


Fig. 5 Analysis of the axon initial segment in excitatory and inhibitory neurons. **a** Representative images of excitatory and inhibitory hippocampal neurons (16 DIV) stained with DAPI (blue), AnK G (red), and PanNa_v (yellow). Cell bodies are circled. Scale bar, 20 μM. **b, c** Representative fluorescence intensity profiles for AnK G (**b**) and PanNa_v (**c**) immunoreactivity for both conditions with the box plots of the AIS length measured for both stainings in excitatory and inhibitory neurons. **d, e** Box plots of the distance from the cell body of AIS start, maximum, and end as measured for AnK G (**d**) and PanNa_v (**e**) stainings. * $P < 0.05$, ** $P < 0.01$; Mann-Whitney U test ($n = 20$ coverslips for both inhibitory and excitatory from 3 independent experiments)

namely it is a retrospective approach, not allowing to know the nature of the neuron in real time during recording and is very time-consuming and unsuitable for large sample numbers. Alternatively, cultures of hippocampal neurons can be prepared from transgenic mice/rats genetically modified to express fluorescent markers in a specific neuronal subtype. An example of this approach is the GAD67 knock-in mouse used in the present work. However, this model shows serious limitations because of the expression of GAD67 also in Prox1-positive granule cells as previously demonstrated [12]. Thus, our goal has been to perform a detailed electrophysiological analysis of the passive and active intrinsic properties of hippocampal neurons that allow an easy and rapid identification of the excitatory or inhibitory nature of the neuron under patch.

The increased resolution afforded by whole-cell patch-clamp recording techniques allows the precise estimation of the passive membrane properties that are normally evaluated at the beginning of each electrophysiological recording. A large body of experimental evidence accumulated in the last 50 years has demonstrated that the resting conductance and potential of inhibitory interneurons deviated markedly from their excitatory cell counterparts [32–36]. However, it is often difficult to get a correct measure of these parameters, in particular for V_m , where small changes in the intracellular/extracellular solution composition, and/or recording quality and resolution often alter ion reversal potentials and passive channel conductance, making the measurement of a “true” V_m problematic. Accordingly, we observed a too wide variability in the passive membrane properties for being useful for distinguishing the two neuronal subpopulations.

Similarly to the passive membrane properties, also the active firing properties are known to differ considerably among excitatory and inhibitory neurons of the mammalian brain [37]. However, due to the extreme heterogeneity, most of these parameters (see Table 1) were not useful for a clear identification. Indeed, interneurons have generally narrower spikes than glutamatergic neurons. However, due to the large variability of individual values, rising slopes, repolarizing slopes, AP peak, AP height, or AHP area that even if significantly different between the two subpopulations did not show enough separation to become a reliable population marker.

The only parameter showing a sharp separation between excitatory and inhibitory neurons was the half-width of the AP, which integrates all the differences observed in the rising and repolarizing kinetics. However, caution should be taken when using only AP half-width to broadly distinguish excitatory and inhibitory neurons. Indeed, in the motor cortex, a major class of inhibitory neurons (low-threshold spiking somatostatin-positive) show an AP half-width intermediate between the two main types of excitatory pyramidal neurons (corticospinal and crossed-corticostriatal) [38]. Thus, studies that split neurons into “putative inhibitory” and “putative excitatory” using only the AP half-width could tend to erroneously group non-fast-spiking inhibitory neurons into the “putative excitatory” population.

The shape of the single AP was further investigated by studying the membrane voltage change (i.e., the first derivative dV/dt) vs voltage that exhibits two-component increase rate during spike generation. Notably, the first steep component of APs (“kink” [22] of GABAergic interneurons is characterized by a clearly increased steepness compared to excitatory neurons. This parallels the more negative voltage threshold, suggesting a change in the localization of VGNaChs at the AIS.

VGNaChs are localized at the AIS through interactions with the scaffolding protein AnK G [27, 28], and indeed, their accumulation at this level makes it the lowest threshold site for AP initiation [23]. Thus, we asked whether the effect that we observed on the “kink” was associated with a different organization of AIS in excitatory and inhibitory neurons. However, the small decrease in the AIS length observed in inhibitory neurons does not correlate with their increased “kink” and more negative voltage threshold, and probably reflects different pattern of voltage-gated channels expressed at the AIS.

The use of the firing frequency as a distinctive criterion to identify excitatory and inhibitory neurons is based on the notion that the firing pattern of a neuron, which includes firing frequency as a function of stimulus strength, bursting vs non-bursting activity and adapting vs non-adapting behavior, is probably a more important physiological property than the shape of the spike. It is generally accepted that inhibitory neurons fire more quickly in response to current injection compared to excitatory neurons. However, this assumption is undermined by the existence of numerous interneurons subclasses that deviate from the typical “fast-spiking” behavior without obvious frequency adaptation (i.e., no change in inter-spike interval) typical of the PV-expressing interneurons [17]. For example, some hippocampal interneurons show considerable spike frequency adaptation (with increasing inter-spike intervals) that limits maximal firing frequencies to levels much lower than those in fast-spiking cells [17]. At the same time, a low percentage of interneurons can also exhibit a variety of spiking phenotypes, including single APs discharged

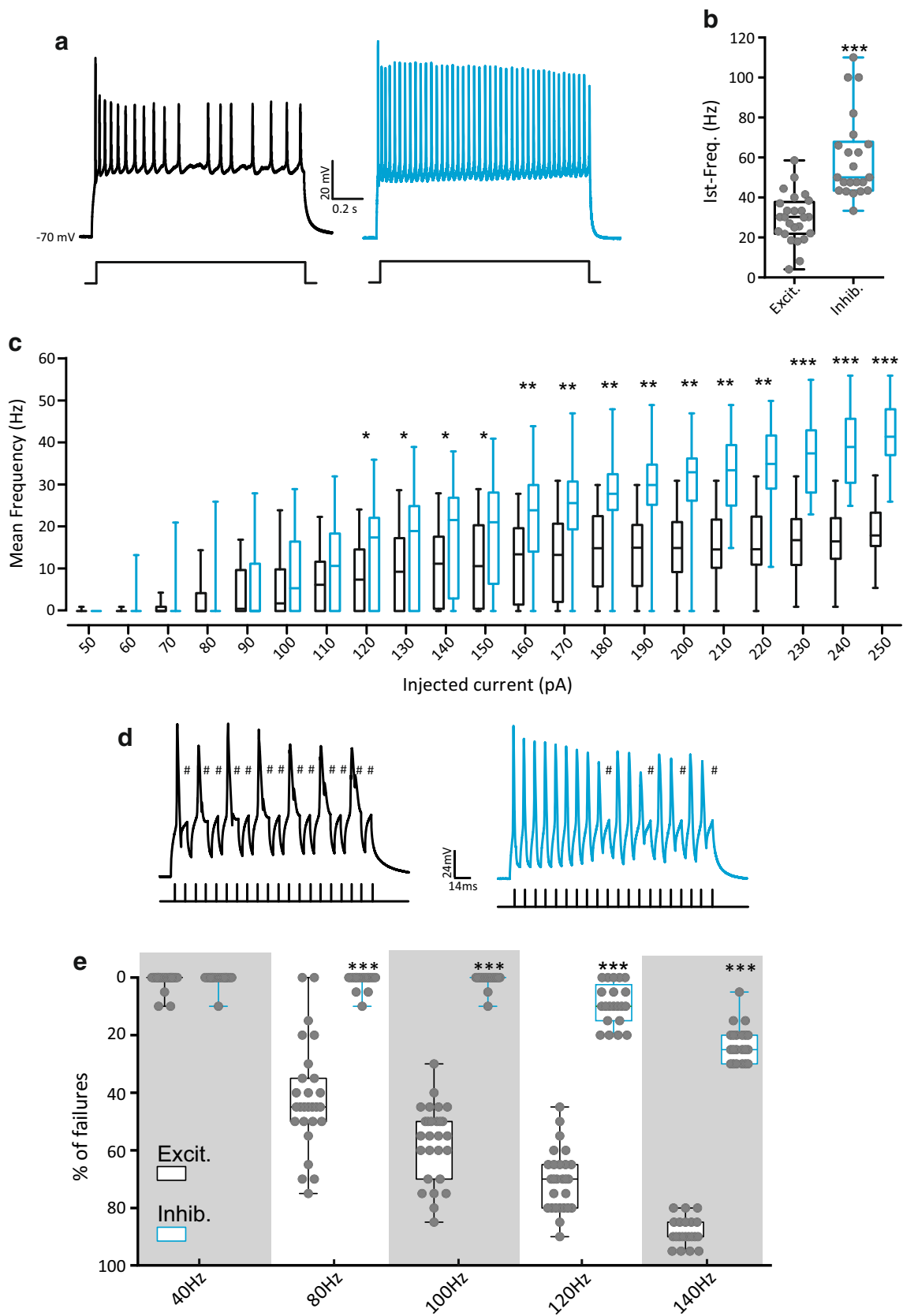


Fig. 6 Firing frequency in excitatory and inhibitory neurons. **a, b** Representative whole-cell current-clamp traces of APs evoked by the injections of 250 pA step current (*inset*) (**a**) and box plot of the instantaneous firing frequency (**b**) in excitatory (*black*) and inhibitory (*blue*) neurons. **c** Box plots of the mean firing frequency vs injected current recorded in excitatory (*black*) and inhibitory (*blue*) neurons in response to a family of injected current steps from 50 to 250 pA (10 pA current increase). **d** Representative recordings of 20 APs evoked by 5-ms current step injection at 120 Hz. Failures are labeled with #. **e** Box plots of the probability to evoke APs at increasing frequencies of current injection in excitatory and inhibitory neurons. The amount of injected current was defined as the minimal current able to evoke 100% of APs at 10 Hz increased by 100 pA. *** $P < 0.001$, non-parametric Mann-Whitney U test ($n = 30$ cells for both conditions)

randomly (*irregular*), short AP trains discharged at high frequency at the beginning of the depolarizing pulse followed by silence (*bursting*) or clusters of spikes separated by unpredictable periods of silence (*stuttering*). This heterogeneity explains why the commonly used parameters, such as mean firing frequency vs injected current plots, do not allow a clear separation of inhibitory from excitatory neurons. However, our results demonstrate that it is possible to overcome this heterogeneity by using a stimulation train of brief and strong current pulses that bring back after each stimulus, the holding potential to a hyperpolarized value, greatly attenuating the effect of the AP adaptation. This protocol amplifies the effect of the narrower spikes of the interneurons that are capable of firing at high frequencies with little decrease in frequency during prolonged stimulation train. The difference between excitatory and inhibitory neurons became particularly relevant at higher stimulation frequencies (> 80 Hz), where this protocol turns out to be undoubtedly the best and faster approach to identify the exact neuronal nature.

In conclusion, all the passive properties and most of the spike-related electrophysiological properties that are conventionally measured and generally believed to be a useful means to distinguish excitatory from inhibitory neurons did not show an acceptable level of certainty. Instead, our data demonstrate that a very simple protocol based on the injection of a train of short current steps at high frequency is a reliable method to identify excitatory and inhibitory neurons in cultured hippocampal neurons, taking advantage from the online analysis offered by the majority of the patch-clamp acquisition software.

Material and Methods

Animals

GAD67-GFP knock-in mice were generated by inserting the cDNA encoding enhanced GFP into the GAD67 locus in TT2 embryonic stem cells, as described in [5]. Heterozygous GAD67-GFP males were mated with wild-type C57BL/6J

females, and GFP-positive pups were identified at birth through a Dual Fluorescent Protein Flashlight (DFP-1, NIGHTSEA, Lexington, MA USA) and confirmed by genotyping, performed by PCR with the following primers: TR-1b: GGCACAGCTCTCCCTTCTGTTTGC; TR-3: GCTCTCCTTTTCGCGTTCCGACAG; TRGFP-8: CTGCTTGTCGGCCATGATATAGACG. All animals were provided by our institutional animal breeding facility in accordance with the guidelines approved by the local Animal Care Committee of the University of Genova. Experiments used 0–2-day-old pups of either sex. Some control experiments were done using wild-type C57BL/6J mice. All experiments were carried out in accordance with the guidelines established by the European Communities Council (Directive 2010/63/EU of 4 March 2014) and were approved by the Italian Ministry of Health (authorization 73/2014-PR and 1276/2015-PR).

Primary Cultures of Dissociated Hippocampal Neurons

Primary hippocampal neurons were prepared from postnatal GAD67-GFP knock-in mice (P0–P1), as previously described [3, 10]. In brief, hippocampi were dissociated by enzymatic digestion in 0.25% trypsin for 6 min at 37 °C and then triturated with a fire-polished Pasteur pipette [39]. No antimetabolic drugs were added to prevent glia proliferation. The following solutions were used for cell culture preparations: HANKS solution, prepared from HBSS (GIBCO 14170-088; red) supplemented with 10 mM HEPES, 30 mM D-glucose, 5 µg/ml Gentamycin, pH 7.4 with KOH; dissection solution, prepared from HANKS solution supplemented with 10% bovine serum albumin and 6 mM $MgSO_4 \cdot 7H_2O$. Primary hippocampal neurons were plated at low density (100 cells/mm²) on 3.5-cm-diameter Petri dishes (Falcon® 35 mm, 353001) treated for 24 h with poly-L-lysine (0.1 mg/ml; Sigma-Aldrich) in borate buffer (0.1 M). Autaptic neurons were prepared as described previously [40, 41]. Cells were plated at very low density (20 cells/mm²) on microislands (40–300 µm in diameter) obtained by spraying of poly-L-lysine (0.1 mg/mL) in buffer borate (0.1 M) on Petri dishes previously pre-treated with 0.15% agarose. Under these conditions, each Petri showed about 10–20 isolated single autaptic neurons grown on microdrops. Cells were grown in a culture medium consisting of Neurobasal A (Gibco™) supplemented with 2%B-27 (Invitrogen, Italy), 1 mM Glutamax, and 5 µg/ml Gentamycin and maintained at 37 °C in a humidified incubator with 5% CO₂.

FACS Sorting of GAD67-GFP Hippocampal Cells

Flow cytometry was performed using the BD FACS ARIA III (BD Biosciences, San Jose, CA, USA) equipped with a forward scatter photomultiplier tube. Cells were scanned for GFP

with a blue laser (488 nm) and detected by a 530/30 bandpass filter at 4 °C with a 100- μ m nozzle at a rate of 1000 events/s. Instrument calibration was checked daily by using Rainbow Fluorescent Particles (BD Biosciences). Forward scatter area (FSC-A) and side scatter area (SSC-A) were used to exclude debris and cell aggregates; doublets were excluded from the basal cell population by side scatter SSC-W vs SSC-H.

Immunocytochemistry

Immunocytochemistry of cultured hippocampal neurons was performed as previously described [10, 42]. In brief, primary hippocampal cells were fixed after 15 days in vitro (DIV) with 4% paraformaldehyde in 0.1 M phosphate buffer (pH 7.4) for 15 min at room temperature and then washed with phosphate-buffered saline (PBS). Cells were then permeabilized with Triton X-100 (0.1%) for 5 min and blocked for 30 min in PBS containing 2% bovine serum albumin (BSA), before their incubation for 24 h with primary antibodies in PBS/3% BSA. For immunofluorescence analysis, neurons were immunostained with antibodies against MAP2 (1:300, Guinea Pig Cat. No. 188004 Synaptic System), GAD67 (1:500, MAB5406 Millipore), and Prox1 (1:300, Rabbit ab101851, ABCam). All images used for quantification of the immunofluorescence intensity were acquired with an Olympus BX41 microscope equipped with $\times 20$ air objective (UPInaFI; NA 0.50) and 1024 \times 1024 pixel (1 pixel = 0.24 μ m) CCD camera (Retiga eExi 28174, Q Imaging). Fluorescence intensity of the UV source (Olympus, X-Cite Series 120; 120 W lamp) and exposure time (50 ms) were maintained constant throughout. The intensity of the endogenous GFP fluorescence was measured by drawing regions of interest (ROIs) in the inner part of the neuronal cell body to avoid the contamination with the fluorescence emitted by GAD67-GFP-positive processes and puncta (putative GABAergic synapses) reaching the GAD67-GFP-negative cell bodies.

Analysis of the Axon Initial Segment

Immunofluorescence of the axon initial segment (AIS) was performed as previously described [41, 43]. For the morphological identification of the AIS, neurons were fixed at 15 DIV and probed with anti-PanNa_v (1:100, mouse Sigma-Aldrich s8809) and anti-Ankyrin G (1:200, rabbit Santa Cruz SC-28561) antibodies. To quantify the immunofluorescence intensity at the AIS, images of cultured neurons were acquired with a Leica SP8 confocal microscope using a 63 \times oil objective and 1024 \times 1024 pixels (1 pixel = 0.24 μ m) in z-stack with 0.3 μ m steps. To analyze stack images, a MATLAB script freely available at www.mathworks.com/matlabcentral/fileexchange/28181-ais-quantification was used as previously described [10, 43, 44]. Briefly, a line profile was drawn along the fluorescently labeled AIS from

the soma through and 5 μ m past the AIS. Pixel fluorescence intensity values were averaged over a 3 \times 3 pixel square centered on an arbitrarily drawn line, which was then smoothed using a 40-point sliding mean and normalized between 1 and 0 (maximum and minimum fluorescence intensity). The maximum position of the AIS was determined where the smoothed and normalized profile of fluorescence intensity reached its peak. The start and end positions of the AIS were the proximal and distal sites, respectively, at which the profile decreased to 33% of its peak. The distance of start, maximum, and end positions of the AIS from the soma was measured, by transmitted light, as the distance from the point where the neuronal process forming the axon had a diameter lower than 2 μ m.

Patch-Clamp Recordings

Whole-cell patch-clamp recordings were conducted on low-density and autaptic hippocampal neurons. Electrophysiological experiments were performed at 12–15 div. Patch pipettes, prepared from thin borosilicate glass (Kimble, Kimax, Mexico), were pulled and fire-polished to a final resistance of 3–4 M Ω when filled with standard internal solution. All recordings were performed at 22–24 °C. The external solution composition was (in mM) 140 NaCl, 2 CaCl₂, 1 MgCl₂, 4 KCl, 10 glucose, and 10 HEPES (pH 7.3 with NaOH). For current-clamp recordings of the firing activity and voltage-clamp recordings of evoked excitatory postsynaptic currents (eEPSCs), the internal solution contained (in mM) 126 K gluconate, 4 NaCl, 1 MgSO₄, 0.02 CaCl₂, 0.1 BAPTA, 15 glucose, 5 HEPES, 3 ATP, and 0.1 GTP (pH 7.2 with KOH). For voltage-clamp recordings of evoked inhibitory postsynaptic currents (eIPSCs), we adopted an internal solution containing (in mM) 140 KCl, 4 NaCl, 1 MgSO₄, 0.1 EGTA, 15 glucose, 5 HEPES, 3 ATP, and 0.1 GTP (pH 7.2 with KOH). Under this condition, internal and external chloride concentrations were equimolar, shifting the chloride reversal potential from a negative value to 0 mV. This experimental configuration, that transforms eIPSCs in inward currents, is typically used for increasing the amplitude of the eIPSCs, evoked at negative holding potentials.

Patch-clamp recordings with leak currents > 200 pA or series resistance > 20 M Ω were discarded. Data acquisition was performed using PatchMaster program (HEKA Elektronik). Series resistance (R_s) was compensated 80% (2 μ s response time) and the compensation was readjusted before each stimulation. The shown potentials were not corrected for the measured liquid junction potential (9 mV).

Voltage clamp was used to record evoked excitatory and inhibitory postsynaptic currents (eEPSCs/eIPSCs), clamping the autaptic neuron at –70 mV and stimulating with two short (0.5 ms) voltage steps to +40 mV applied at 50 ms interval. For each couple of ePSCs, the ratio I₂/I₁ (paired-pulse ratio, PPR) was calculated, where I₁ and I₂ are the amplitudes of the

ePSCs evoked by the conditioning and test stimuli, respectively. The amplitude of I2 was determined as the difference between the I2 peak and the corresponding value of I1 calculated by mono-exponential fitting of the ePSC decay. PPR is particularly useful to immediately identify excitatory synapses that show $PPR > 1$, from inhibitory synapses that show $PPR < 1$.

Synaptic currents were acquired in isolated autaptic neurons at 20 kHz and low-pass filtered at 4 kHz. The electrophysiological phenotypes of autaptic neurons under study were identified using the positivity to GFP fluorescence and confirmed by visual analysis of the current kinetics and by using specific blockers of excitatory (CNQX, 10 μ M) and inhibitory (BIC, 30 μ M) synaptic transmission.

Current-clamp recordings of the firing activity of low-density and autaptic hippocampal neurons were sampled at 50 kHz and low-pass filtered at 10 kHz using an external solution supplemented with 10 μ M CNQX or 30 μ M BIC. The following parameters were studied:

- Resting membrane potential (V_{rest}) was determined immediately after breaking the membrane and establishing the whole-cell mode. It was not corrected for a junction potential of 11 mV;
- Input resistance (R_{in}) was calculated in a linear region of the voltage-current relationship centered at the holding potential (-70 mV), through the injection of hyperpolarizing and depolarizing current steps (-20 , -10 , 10 , 20 pA);
- Neuronal firing activity was induced by injection of 10 pA current steps lasting 1 s from a holding potential of -70 mV maintained through a constant current injection;
- The mean firing frequency of each current step was calculated by dividing the number of APs-1 by the time interval (in s) between the first and the last evoked AP;
- The instantaneous firing frequency, calculated at maximal value of injected current (250 pA), was estimated as the reciprocal value of the time difference between the first 2 evoked APs [29];
- The percentage of failures was studied using trains of 20 current steps lasting 5 ms, applied at various frequencies (40–140 Hz). The current value used to evoke APs with this protocol was selected as the minimal current able to evoke an AP for each step of the train at 10 Hz (0% of failures), increased by 100 pA;
- The half-width was calculated at half maximal AP height. The AP height was defined as the peak relative to the most negative voltage reached during the afterhyperpolarization (AHP) immediately after the spike;
- The afterhyperpolarization (AHP) was determined as the integral of the area comprised between the most negative value reached by the AHP and the baseline level recovered 50 ms after the AHP-negative peak;

- Peak amplitude of action potentials was measured from $V_{threshold}$ to the AP peak.

To study the biophysical properties of the single AP more in depth, the plot of the time derivative of voltage (dV/dt) vs voltage was constructed (phase-plane plot). The plot was obtained from the first AP elicited by the minimal current injection by current-clamp family step protocol and was used to extract the maximum rising slope, the AP peak, the maximum repolarizing slope, and the V threshold. The slope of phase-plots at the AP threshold (“kink”) [22, 26] was calculated using linear regression of the first 10 data points of the rising phase with a Y-value > 4 mV/ms. The voltage threshold was defined as the first voltage value at which dV/dt exceeded 4 mV/ms. Such value was empirically identified as the value offering the higher guarantee to identify the initial voltage change due to Na^+ current activation, without any interference of the voltage change due to the high frequency thermal noise, that affect voltage recordings [45, 46]. The electrophysiological recordings were analyzed using Fit master (HEKA) software. All values describing AP shape represent averages from 10 single action potentials for each cell.

Statistical Analysis

All experiments were replicated at least three times. Data are shown as means \pm SEM or as box plots, with median (line), second and third interquartile ranges (box), and whiskers representing the min and the max values. The F-test was used to compare variance between two sample groups. To compare two normally distributed sample groups, the unpaired Student’s two-tailed t test was used. To compare two sample groups that were not normally distributed, the Mann-Whitney’s U test was used. To compare more than two normally distributed experimental groups, one-way ANOVA followed by the Tukey’s multiple comparison test was used. Alpha levels for all tests were 0.05% (95% confidence intervals). Statistical analysis was carried out using OriginPro-8 (OriginLab Corp., Northampton, MA, USA) and Prism (GraphPad Software, Inc.) software.

Funding Information This study was supported by research grants from the Compagnia di San Paolo Torino (ID ROL 20612 and 9344); Ministero della Salute Ricerca Finalizzata (GR-2016-02363972); EU Era-Net Neuron 2017 “Snaropathies” and ITN “ECMED” (Grant agreement n. 642881).

Compliance with Ethical Standards

All experiments were performed in accordance with the guidelines established by the European Communities Council (Directive 2010/63/EU of September 22, 2010) and were approved by the Italian Ministry of Health.

Conflict of Interest The authors declare that they have no competing interests.

Publisher's Note Springer Nature remains neutral with regard to jurisdictional claims in published maps and institutional affiliations.

References

- Wiltgen BJ, Brown RA, Talton LE, Silva AJ (2004) New circuits for old memories: the role of the neocortex in consolidation. *Neuron* 44:101–108. <https://doi.org/10.1016/j.neuron.2004.09.015>
- Kaech S, Banker G (2006) Culturing hippocampal neurons. *Nat Protoc* 1:2406–2415. <https://doi.org/10.1038/nprot.2006.356>
- Beaudoin GM 3rd, Lee SH, Singh D, Yuan Y, Ng YG, Reichardt LF, Arikath J (2012) Culturing pyramidal neurons from the early postnatal mouse hippocampus and cortex. *Nat Protoc* 7:1741–1754. <https://doi.org/10.1038/nprot.2012.099>
- Tóth K, McBain CJ (2000) Target-specific expression of pre- and postsynaptic mechanisms. *J Physiol* 525:41–51. <https://doi.org/10.1111/j.1469-7793.2000.00041.x>
- Tamamaki N, Yanagawa Y, Tomioka R, Miyazaki J, Obata K, Kaneko T (2003) Green fluorescent protein expression and colocalization with calretinin, parvalbumin, and somatostatin in the GAD67-GFP knock-in mouse. *J Comp Neurol* 467:60–79. <https://doi.org/10.1002/cne.10905>
- Sahara S, Yanagawa Y, O'Leary DD, Stevens CF (2012) The fraction of cortical GABAergic neurons is constant from near the start of cortical neurogenesis to adulthood. *J Neurosci* 3:4755–4761. <https://doi.org/10.1523/JNEUROSCI.6412-11.2012>
- Ono M, Yanagawa Y, Koyano K (2005) GABAergic neurons in inferior colliculus of the GAD67-GFP knock-in mouse: electrophysiological and morphological properties. *Neurosci Res* 51:475–492. <https://doi.org/10.1016/j.neures.2004.12.019>
- Suzuki N, Bekkers JM (2010) Distinctive classes of GABAergic interneurons provide layer-specific phasic inhibition in the anterior piriform cortex. *Cereb Cortex* 20:2971–8420. <https://doi.org/10.1093/cercor/bhq046>
- Suzuki N, Bekkers JM (2010) Inhibitory neurons in the anterior piriform cortex of the mouse: classification using molecular markers. *J Comp Neurol* 518:1670–1687. <https://doi.org/10.1002/cne.22295>
- Valente P, Orlando M, Raimondi A, Benfenati F, Baldelli P (2016) Fine tuning of synaptic plasticity and filtering by GABA released from hippocampal autaptic granule cells. *Cereb Cortex* 26:1149–1167. <https://doi.org/10.1093/cercor/bhu301>
- Safiulina VF, Fattorini G, Conti F, Cherubini E (2006) GABAergic signaling at mossy fiber synapses in neonatal rat hippocampus. *J Neurosci* 26:597–608. <https://doi.org/10.1523/JNEUROSCI.4493-05.2006>
- Gutiérrez R (2009) The dual glutamatergic/GABAergic phenotype of hippocampal granule cells. *Trends Neurosci* 28:297–303. <https://doi.org/10.1016/j.tins.2005.04.005>
- Gutiérrez R, Romo-Parra H, Maqueda J, Vivar C, Ramirez M, Morales MA, Lamas M (2003) Plasticity of the GABAergic phenotype of the glutamatergic granule cells of the rat dentate gyrus. *J Neurosci* 23:5594–5598. <https://doi.org/10.1523/JNEUROSCI.23-13-05594.2003>
- Lavado A, Lagutin OV, Chow LML, Baker SJ, Oliver G (2010) Prox1 is required for granule cell maturation and intermediate progenitor maintenance during brain neurogenesis. *PLoS Biol* 8:e1000460. <https://doi.org/10.1371/journal.pbio.1000460>
- Acuna-Goycolea C, Tamamaki N, Yanagawa Y, Obata K, van den Pol AN (2005) Mechanisms of neuropeptide Y, peptide YY, and pancreatic polypeptide inhibition of identified green fluorescent protein-expressing GABA neurons in the hypothalamic neuroendocrine arcuate nucleus. *J Neurosci* 25:7406–7419. <https://doi.org/10.1523/JNEUROSCI.1008-05.2005>
- Brown RE, McKenna JT, Winston S, Basheer R, Yanagawa Y, Thakkar MM, McCarley RW (2008) Characterization of GABAergic neurons in rapid-eye-movement sleep controlling regions of the brainstem reticular formation in GAD67-green fluorescent protein knock-in mice. *Eur J Neurosci* 27:352–363. <https://doi.org/10.1111/j.1460-9568.2008.06024.x>
- Pelkey KA, Chittajallu R, Craig MT, Tricoire L, Wester JC, McBain CJ (2017) Hippocampal GABAergic inhibitory interneurons. *Physiol Rev* 97:1619–1747. <https://doi.org/10.1152/physrev.00007.2017>
- Milior G, Di Castro MA, Pepe' Sciarria L, Garofalo S, Branchi I, Ragozzino D, Limatola C, Maggi L (2016) Electrophysiological properties of CA1 pyramidal neurons along the longitudinal axis of the mouse hippocampus. *Sci Rep* 6:38242. <https://doi.org/10.1038/srep38242>
- Pedroni A, Minh D, Mallamaci A, Cherubini E (2014) Electrophysiological characterization of granule cells in the dentate gyrus immediately after birth. *Front Cell Neurosci* 8:44. <https://doi.org/10.3389/fncel.2014.00044>
- Stuart G, Schiller J, Sakmann B (1997) Action potential initiation and propagation in rat neocortical pyramidal neurons. *J Physiol* 505:617–632
- Palmer LM, Stuart GJ (2006) Site of action potential initiation in layer 5 pyramidal neurons. *J Neurosci* 26:1854–1863. <https://doi.org/10.1523/JNEUROSCI.4812-05.2006>
- Shu Y, Yu Y, Yang J, McCormick DA (2007) Selective control of cortical axonal spikes by a slowly inactivating K⁺ current. *Proc Natl Acad Sci U S A* 104:11453–11458. <https://doi.org/10.1073/pnas.0702041104>
- Kole MH, Stuart GJ (2008) Is action potential threshold lowest in the axon? *Nat Neurosci* 11:1253–1255. <https://doi.org/10.1038/nn.2203>
- Yu Y, Shu Y, McCormick DA (2008) Cortical action potential backpropagation explains spike threshold variability and rapid-onset kinetics. *J Neurosci* 28:7260–7272. <https://doi.org/10.1523/JNEUROSCI.1613-08.2008>
- McCormick DA, Shu Y, Yu Y (2007) Neurophysiology: Hodgkin and Huxley model — still standing? *Nature* 445:E1–E2. <https://doi.org/10.1038/nature05523>
- Naundorff B, Wolf F, Volgushev M (2006) Unique features of action potential initiation in cortical neurons. *Nature* 440:1060–1063. <https://doi.org/10.1038/nature04610>
- Garrido JJ, Giraud P, Carlier E, Fernandes F, Moussif A, Fache MP, Debanne D, Dargent B (2003) A targeting motif involved in sodium channel clustering at the axonal initial segment. *Science* 300:2091–2094. <https://doi.org/10.1126/science.1085167>
- Pan Z, Kao T, Horvath Z, Lemos J, Sul JY, Cranstoun SD, Bennett V, Scherer SS et al (2006) A common ankyrin-G-based mechanism retains KCNQ and NaV channels at electrically active domains of the axon. *J Neurosci* 26:2599–2613. <https://doi.org/10.1523/JNEUROSCI.4314-05.2006>
- Kole MHP, Stuart GJ (2012) Signal processing in the axon initial segment. *Neuron* 73:235–247. <https://doi.org/10.1016/j.neuron.2012.01.007>
- Yoshimura T, Rasband MN (2014) Axon initial segments: diverse and dynamic neuronal compartments. *Curr Opin Neurol* 27:96–102. <https://doi.org/10.1016/j.conb.2014.03.004>
- Bean BP (2007) The action potential in mammalian central neurons. *Nat Rev Neurosci* 8:451–465. <https://doi.org/10.1038/nm2148>

32. Traub RD, Miles R (1992) Neuronal networks of the hippocampus. Cambridge University Press 82:394–395 doi:[https://doi.org/10.1016/0013-4694\(92\)90012-7](https://doi.org/10.1016/0013-4694(92)90012-7)
33. Traub RD, Miles R, Wong RK (1989) Model of the origin of rhythmic population oscillations in the hippocampal slice. *Science* 10: 1319–1325. <https://doi.org/10.1126/science.2646715>
34. Kawaguchi Y, Hama K (1988) Physiological heterogeneity of nonpyramidal cells in rat hippocampal CA1 region. *Exp Brain Res* 72:494–502. <https://doi.org/10.1007/BF00250594>
35. Lacaille JC, Mueller AL, Kunkel DD, Schwartzkroin PA (1987) Local circuit interactions between oriens/alveus interneurons and CA1 pyramidal cells in hippocampal slices: electrophysiology and morphology. *J Neurosci* 7:1979–1993. <https://doi.org/10.1523/JNEUROSCI.07-07-01979.1987>
36. Lacaille JC, Schwartzkroin PA (1988) Stratum lacunosum-moleculare interneurons of hippocampal CA1 region. II. Intracellular and intradendritic recordings of local circuit synaptic interactions. *J Neurosci* 8:1411–1424. <https://doi.org/10.1523/JNEUROSCI.08-04-01411.1988>
37. Connors BW, Gutnick MJ (1990) Intrinsic firing patterns of diverse neocortical neurons. *Trends Neurosci* 13:99–104. [https://doi.org/10.1016/0166-2236\(90\)90185-D](https://doi.org/10.1016/0166-2236(90)90185-D)
38. Suter BA, Migliore M, Shepherd GM (2013) Intrinsic electrophysiology of mouse corticospinal neurons: a class-specific triad of spike-related properties. *Cereb Cortex* 23:1965–1977. <https://doi.org/10.1093/cercor/bhs184>
39. Banker G, Goslin K (1998) *Culturing nerve cells*, 2nd edn. MIT Press, Cambridge MA, pp. 339–370
40. Chiappalone M, Casagrande S, Tedesco M, Valtorta F, Baldelli P, Martinoia S, Benfenati F (2009) Opposite changes in glutamatergic and GABAergic transmission underlie the diffuse hyperexcitability of synapsin I deficient cortical networks. *Cereb Cortex* 19:1422–1439. <https://doi.org/10.1093/cercor/bhn182>
41. Valente P, Casagrande S, Nieuwenhuis T, Verstegen AMJ, Valtorta F, Benfenati F, Baldelli P (2012) Site-specific synapsin I phosphorylation participates in the expression of post-tetanic potentiation and its enhancement by BDNF. *J Neurosci* 32:5868–5879. <https://doi.org/10.1523/JNEUROSCI.5275-11.2012>
42. Glynn MW, McAllister AK (2006) Immunocytochemistry and quantification of protein colocalization in cultured neurons. *Nat Protoc* 1:1287–1296. <https://doi.org/10.1038/nprot.2006.220>
43. Fruscione F, Valente P, Sterlini B, Romei A, Baldassari S, Fadda M, Prestigio C, Giansante G et al (2018) PRRT2 controls neuronal excitability by negatively modulating Na⁺ channel 1.2/1.6 activity. *Brain* 141:1000–1016. <https://doi.org/10.1093/brain/awy051>
44. Grubb MS, Burrone J (2010) Activity-dependent relocation of the axon initial segment fine-tunes neuronal excitability. *Nature* 465: 1070–1074. <https://doi.org/10.1038/nature09160>
45. Valente P, Lignani G, Medrihan L, Bosco F, Contestabile A, Lippiello P, Ferrea E, Schachner M et al (2016) Cell adhesion molecule L1 contributes to neuronal excitability regulating the function of voltage-gated Na⁺ channels. *J Cell Sci* 129:1878–1891. <https://doi.org/10.1242/jcs.182089>
46. Platkiewicz J, Brette R (2010) A threshold equation for action potential initiation. *PLoS Comput Biol* 6(7):e1000850. <https://doi.org/10.1371/journal.pcbi.1000850>